Acoustic resonances in a 3D open cavity: comparison of experimental and numerical results.

Santiago Ortiz[a)]
Pedro Cobo[b)]
Centro de Acústica Aplicada y Evaluación No Destructiva (CAEND), CSIC, Serrano 144, 28006 Madrid (Spain).

Leo González[c)]
Escuela de Ingeniería Naval, Universidad Politécnica de Madrid, Plaza Cardenal Cisneros, 28040 Madrid (Spain)

Daniel Rodríguez[d)]
Vassilios Theofilis[e)]
School of Aerospace Engineering, Universidad Politécnica de Madrid, Plaza Cardenal Cisneros, 28040 Madrid (Spain)

Airframe noise is as significant a component of the total noise radiated by an aircraft on approach as that of the other main source, jet noise. Of the various sources of airframe noise, the landing gear cavity has been identified as a potential radiator of high-level resonant tones. Although these tones are generated as the result of a complex interaction of the turbulent air flow with the cavity, it is expected that the acoustic resonances of the cavity approach the noise tones at low Mach numbers. Moreover, an accurate design of noise control systems of these cavity tones can be facilitated by advance knowledge of the acoustic resonances of the open cavity. The present work compares two theoretical methods to predict the acoustic resonances of a 3D open cavity. The first one solves the multi-dimensional Helmholtz equation closed with appropriate Perfectly Matched Layer absorbing boundary conditions. The second one runs in the time domain and models the time response at any point of the cavity as a sequence of attenuated and delayed impulses coming, the first from the real, and the subsequent from the mirror imaged sources (Image

[a)] email: santiago.ortiz@caend.upm-csic.es
[b)] email: pcobo@caend.upm-csic.es
[c)] email: leo.gonzales@upm.es
[d)] email: dani@torroja.dmt.upm.es
[e)] email: vassilios.theofilis@upm.es

Source Model). Preliminary work with two-dimensional (rectangular) open cavities has delivered excellent comparisons between the two sets of theoretical results, as well as with those of experiments performed. Predictions of the two methods in the present three-dimensional cavity configuration are planned, the results of which will be compared with experimental measurements in a three-dimensional (cubic) open cavity.

1 INTRODUCTION

Aerodynamical noise is omnipresent in the context of air and ground transportation, penalizing the acoustic comfort inside airplanes and vehicles, and increasing the environmental noise in the vicinity of airports. Wheel wells compartments are sources of high level cavity tones during landing and takeoff airplane operations. The fundamental mechanisms underlying the coupling between the flow instability and the underneath open cavity have been elucidated by many investigators[1-5]. Several researches have reported numerical methods to provide the eigenvalues (resonant frequencies) and eigenfunctions (normal modes) of open cavities without flow. More recently, Koch[6] and Hein et al.[7] proposed to find the acoustic resonances of 2D and 3D rectangular open cavities by solving the Helmholtz wave equation by high order finite-element methods. This method provides the resonant frequencies and the normal modes of the open cavity and needs to implement absorbing conditions (PML) at the boundaries of the numerical domain to avoid unphysical reflections at such computational boundaries. Therefore, this method results to be high-demanding from a computational point of view.

The main objective of this work is to compare this Helmholtz-PML method with a faster, less-demanding and efficient method to reveal the acoustic resonances and modes of an open cavity. As usually done in Room Acoustics, the method provides the time response of any source-microphone pair through the convolution between the cavity impulse response with the loudspeaker time waveform[8]. The impulse response of the cavity is obtained by the application of the Image Source Method[9-10]. Since this method proceeds in the time domain, absorbing boundary conditions are not needed. Furthermore, since time responses at any point inside the cavity are modeled, a direct comparison with measurements can straightforwardly be carried out.

The layout of the paper is as follows. Section 2 re-examines the Helmholtz with PML method. In Section 3, the main features of the ISM are reviewed. Section 4 describes the 3D cubic open cavity built for numerical/experimental comparison, as well as the measurement procedure. Section 5 provides experimental validation of numerical predictions. Concluding remarks are given in Section 6.

2 COMPUTATIONAL MODEL AND NUMERICAL IMPLEMENTATION.

The Helmholtz equation has been assumed as the representing model of the acoustic phenomena.

$$\nabla^2\phi + \lambda^2\phi = 0 \quad . \tag{1}$$

In this context $\phi(x, y)$ is the potential velocity and λ is a non-dimensional frequency given by the expression:

$$\lambda = \frac{\omega^* D}{c^*_{ref}} \quad . \tag{2}$$

All lengths will be non-dimensionalized with characteristic reference length W, velocities with the ambient speed of sound c^*_{ref}, densities with the ambient density ρ^*_0, and pressures $\rho^*_{ref}(c^*_{ref})^2$. Equation (1) represents a typical eigenvalue problem where λ^2 is the calculated eigenvalue and $\phi(x,y)$ the corresponding eigenvector.

2.1 Boundary conditions

To simulate the presence of an open boundary and the radiation of energy to the infinity, a nonreflecting or absorbing boundary condition has been implemented. This kind of boundary condition absorbs the outgoing energy without unphysical wave reflections. Here a PML boundary condition has been chosen as a preferred method to overcome this difficulty[6,11]. A computational sub-domain where the Perfectly Matched Layer (PML) boundary conditions take place will be required. According to this, two sub-domains can be distinguished, first the physical domain Ω_{phys} and second the necessary extension to implement the PML boundary condition Ω_{PML}. The last domain Ω_{PML} is described in this geometry by the dimensions d_x, d_y and d_z in the directions x, y and z respectively.

The inner boundary described by the cavity geometry will have Neumann type boundary condition, that implies zero derivative in the normal direction $\delta\phi/\delta n = 0$. The rest of the boundary represents an artificial limit imposed by the fact of having a finite domain.

The structure of the new dumping functions $\sigma_x(x)$, $\sigma_y(y)$ and $\sigma_z(z)$ are chosen in such that have zero value at the internal physical domain interface , $x_0 = \pm 1$ in the x direction; and $y_0 = 0.5$ in the y direction and $z_0 = \pm 1$, and also have a smooth potential growth towards the open boundary such as:

$$\sigma_x(x) = \begin{cases} \sigma_{0,x}(x - x_0)^\beta & x > x_0 \\ 0 & |x| \le x_0 \\ -\sigma_{0,x}(-x - x_0)^\beta & x \le -x_0 \end{cases} \quad \sigma_y(y) = \begin{cases} \sigma_{0,y}(y - y_0)^\beta & y > y_0 \\ 0 & |y| \le y_0 \end{cases} \quad \sigma_z(z) = \begin{cases} \sigma_{0,z}(z - x_0)^\beta & z > z_0 \\ 0 & |z| \le z_0 \\ -\sigma_{0,z}(-z - z_0)^\beta & z \le -z_0 \end{cases}, \qquad (3)$$

where $\sigma_{0,x}$, $\sigma_{0,y}$ and $\sigma_{0,z}$ are the dumping coefficients and β is a shape parameter. In our case, we used β=1. As $\sigma_{0,x} = \sigma_{0,y} = \sigma_{0,z}$ we will refer to them as σ hereinafter.

Using similar arguments as in Koch[6], homogeneous Dirichlet boundary conditions at the external boundary of the PML sub-domain, this is $x = \pm(x_0 + 1)$, $y = y_0 + 1$ and $z = \pm(z_0 + 1)$.

The spatial discretization of the Helmholtz equation has been done using a second order finite element discretization and tetrahedral elements. For the solution of the generalized eigenvalue problem derived from the finite element discretization an iterative shift and inverse Arnoldi method has been used[12-13].

The accuracy of the numerical solution may be controlled by the following parameters: number of tetrahedral elements N_{el} and the Krylov subspace dimension M of the Arnoldi method. A proper selection of these parameters is crucial for the accuracy of the final results. Mesh and numerical parameters, as N_{el} have been increased until the eigenvalues obtained have

been converged. As expected, we found that by making the Krylov subspace larger we obtained a larger number of physical resonant modes.

We were also able to appreciate that by making σ smaller, the modes contained more numerical noise coming from the PML boundary condition. The range of σ that we used was from 3 to 10, using in some cases a non zero shift parameter. The range of PML boundary condition parameters contain those used by previous authors as Hein *et al.*[7] in 3D cavities. The shift parameter was used in order to accurately approximate the part of the spectrum close to the area where the real part of $\lambda / 2\pi = 1$.

3 EFFICIENT IMAGE SOURCE MODELLING (ISM)

3.1 Sound field inside the cavity

The classical ISM algorithm by Allen and Berkley[9] provides the impulse response of a rectangular room of any length, width, height and reflection characteristics.

A rectangular open cavity can be modelled in the same way using the ISM by considering five walls perfectly rigid except for one which absorbs the incident sound completely. Compared to a closed room, the image space consists of only two levels as the opening of the cavity generates no images, Fig. 1, although the actual image space is three-dimensional, a two-dimensional view is illustrated for the sake of clarity.

The original[9] equation to obtain the pressure time response for a point source S=(x,y,z) and receiver R=(x',y',z') inside a closed room is:

$$p(t,S,R) = \sum_{q=0}^{1}\sum_{j=0}^{1}\sum_{k=0}^{1}\sum_{n=-\infty}^{\infty}\sum_{l=-\infty}^{\infty}\sum_{m=-\infty}^{\infty} \beta x_1^{|n-q|}\beta x_2^{|n|}\beta y_1^{|l-j|}\beta y_2^{|l|}\beta z_1^{|m-k|}\beta z_2^{|m|} \times \frac{\delta\left|t-\left(\left|r_p+r_r\right|/c\right)\right|}{4\pi\left|r_p+r_r\right|}, \tag{4}$$

where the β's, are the reflection coefficients at the six boundaries, $r_p = (x - x' + 2qx', y - y' + 2jy', z - z' + 2kz')$, where (x, y, z) is the vector source position, (x', y', z') is the vector receiver location, (q, j, k) is an integer three vector, and $r_r = 2\left(nL_x, lL_{y,} mL_z\right)$, where (L_x, L_y, L_z) are the room dimensions and (n, l, m) is the integer vector triplet for higher order reflections.

In the case of an open cavity, opened at the top, the reflection coefficient $\beta_{y_2}^{|m|}$ and the sum over m orders of reflection is limited to only two values: -1 and 0. Therefore Eq. (4), can be modified for an open cavity as follows:

$$p(t,S,R) = \sum_{q=0}^{1}\sum_{j=0}^{1}\sum_{k=0}^{1}\sum_{n=-\infty}^{\infty}\sum_{l=-\infty}^{\infty}\sum_{m=-1}^{0} \beta x_1^{|n-q|}\beta x_2^{|n|}\beta y_1^{|l-j|}\beta z_2^{|l|}\beta z_1^{|m-k|} \times \frac{\delta\left|t-\left(\left|r_p+r_r\right|/c\right)\right|}{4\pi\left|r_p+r_r\right|}, \tag{5}$$

where r_p and r_r remain the same as in Eqn. (4).

3.1 Sound field outside the cavity

Unfortunately, when the receiver is placed outside the cavity not all the image sources created with Eq. (5) are valid. Therefore, in order to model the sound field at a receiver point outside, a visibility test has to be done in addition. Figure 2, illustrates an example of three different receiver positions outside the cavity, R_1, R_2 and R_3, and two first order image sources, IS_1 and IS_2. We can see how IS_1 is valid at receivers R_1 and R_2 but not at R_3, as the reflection point is outside the cavities boundaries. The same happens to IS_2 as it is not visible at any of the three receiver positions.

The visibility test implemented in this work is based on the original idea proposed by Mechel[14] where the test examines if a point, P, is inside a polygonal pyramid which is subtended by a wall, W. The method is also similar to frustum tracing[15], where a frustum (pyramidal or volumetric beams) is created from the sound source or image source to find potential visible reflecting planes.

The visibility method implemented here pre-calculates the image source coordinates $IS(x, y, z)$ using Eq. 5. Then, a frustum is created from the receiver point R crossing the four edges of the open side of the cavity $\{e_1, e_2, e_3, e_4\}$, Fig. 3.

All IS that are inside the frustum will be visible from the receiver and all the ones outside will be discarded.

To construct the frustum, the coordinates of the edges of the open surface $\{e_1, e_2, e_3, e_4\}$ and the receiver positions, R, have to be known. Thus, the four sides of the frustum can be defined as follows:

$$\begin{cases} Frust1 = \{R, e_1, e_2\} \\ Frust2 = \{R, e_2, e_3\} \\ \text{Frust3} = \{R, e_3, e_4\} \\ Frust4 = \{R, e_4, e_1\} \end{cases}, \tag{6}$$

where the edges of each plane of the frustum should be ordered so that the normal vector of the plane points to the inside of the cavity.

Calculating the parameters of the normal form of each planes we can test if an $IS(x, y, z)$ is inside, on the plane or outside the plane using the expression:

$$ax + by + cz + d \begin{cases} > 0, \text{ IS inside plane} \\ = 0, \text{ IS in plane} \\ < 0, \text{ IS outside plane} \end{cases}, \tag{7}$$

where a, b, c, and d are the normal form parameters of the plane and (x, y, z) are the coordinates of the IS being checked.

The complete visibility test is done by repetition of the inside check on the four planes forming the frustum. If one of the test is negative the loop can be aborted. The *IS* has to be inside all of the frustum planes in order to be valid.

Only valid image sources are used to calculate the cavity impulse.

4 EXPERIMENTAL VALIDATION

A three-dimensional rectangular open cavity was built to compare the two numerical methods previously described with measurements. This Section describes the cavity, as well as the measurement method to characterize the acoustic field inside it.

4.1 The rectangular open cavity

A wooden 3D open cavity was made with DM wood panels of thickness 3 cm. The open cavity has dimensions (L,D,W)=(53, 38, 32) cm, corresponding to the (x, y, z) axis, Fig. 4. Thus L/ D= 1.4 and W/D= 0.84. A Sonavox Honeycomb loudspeaker (4 ") is set at the centre line of the front wall, with coordinates $(x, y, z) = (26.5, 35, 0)$ cm. Eight ½ inch FONESTAR 2210 electret microphones were used to measure the loudspeaker-microphone time responses in the cavity. The loudspeaker-microphone pair has a non flat frequency response. Therefore, peaks of this non-flat frequency response could be misinterpreted as resonances of the cavity. To avoid that, the loudspeaker response was first equalized by inverse filtering[16].

4.2 Measurement procedure

Time responses between the loudspeaker and microphones located at the points of a grid with $\Delta x = \Delta y = \Delta z = 3.1\,\text{cm}$, Fig. 5, were measured inside the anechoic chamber. Notice that if four points are required to resolve a wavelength, only modes with frequency less than approximately $c/(4\Delta) = 2760$ Hz will be reliably measured, where c is the speed of sound and Δ the measurement grid spacing.

A self-developed Virtual Instrument called MUIRSA was used to measure the time responses between the loudspeaker and the microphones in the cavity. MUIRSA consists of a DAQ NI PCI-MIO-16E card with 8 input channels and two output channels and a maximum sampling frequency of 250 kHz, driven by Matlab. In this case, MUIRSA was configured to acquire the time response between the loudspeaker and eight microphones, sampled at 20 kHz.

The above explained procedure provides the time domain pressure $p(t, r_i)$ radiated by the loudspeaker at each point $r_i = (x_i, y_i, z_i)$ of the measurement grid. From these, the Frequency Response Functions (FRF) between the loudspeaker and the microphones can be easily obtained by:

$$FRF(f, r_i) = 20\log_{10}\left|\Im\{p(t, r_i)\}\right|, \tag{8}$$

where $\Im$ stands for the Fourier transform. The plots of these FRF for a given frequency, f_m, at a plane will image the acoustic field in such a plane, this plot will outline closely the corresponding acoustic mode.

3 RESULTS

The measurement procedure described above has enabled us to identify the different resonant modes and to characterize each of them. The modal frequencies of the cavity are picked up from the peaks of the FRF, Fig. 6 and 7. As it can be seen, there is an excellent correspondence between the experimental and the numerical Image Source Model FRFs, except for some peaks which are observed in the experimental FRF but they are not in the ISM ,marked with red arrows in Fig. 6. These correspond to frequencies of axial modes (m,0,0), with m=0 and 1. While the ISM point source is exactly on a nodal line of these modes, the real one has a size (4 inch) enough to slightly excite them.

3.1 Helmholtz eigenvalue problem results

In order to solve the 3D open cavity a non-structured mesh with $N_{el} = 293045$ tetrahedral elements and 406004 nodes was used. The mesh size inside the cavity was h=0.03. An iterative Arnoldi method (M=500,shift=(0,0)) was used in most of the computations.

The real part of the normalized eigenvalues corresponds with the frequency of the resonant modes while the imaginary part is a measure of the radiation loss. According to this fact, modes with negligible imaginary part compared to the real part correspond to situations where the mode is confined inside the cavity and consequently well captured by the interior microphones. The presence of the radiative modes, with an increasing imaginary part, should be captured by the external microphones. Each resonant mode is noted by three integer number (i,j,k), where i,j,k=0,1,… are the length, depth and width mode numbers inside the cavity corresponding to the x,y and z directions respectively, see Table 1.

3.2 Computational results and comparison with experimental results

Table 2 shows a comparison between the resonant frequencies obtained with the three different methods: Helmholtz eigenvalue problem, ISM simulation and experimental measurements. As can be observed the agreement among them is remarkable.

Finally, let us illustrate some of the revealed normal modes. Figures 8-9 show the 3D representations of the axial modes (0,0,1) and (2,0,0), respectively. Again, an excellent agreement is found between the two numerical and experimental mode representations.

4 DISCUSSION AND CONCLUSIONS

The experiment results and numerical methods presented in this work are in excellent agreement. The Helmholtz-PML method is more precise (maximum error of 2%) compared to Image Source Model (ISM) (maximum error of 4.7%). Nevertheless, whilst the Helmholtz computational method provides the eigenvalues (modal frequencies) and eigenfunctions of the problem more precisely, it requires high computational demands in 3D. The ISM, in the other hand, provides directly the time response between a source and a receiver in the cavity. Fourier transform methods convert this time signal in a frequency response function. Therefore, efficiently and accurately predicting the cavity resonance in any position.

5 ACKNOWLEDGEMENTS

This research was supported by the Spanish Ministry of Economy and Competitiveness through Grants Nº TRA2011-26261-C04-01 and TRA2009-13648.

6 REFERENCES

1. H.E. Plumbee, J.S. Gibson and L.W. Lassiter, "A theoretical and experimental investigation of the acoustic response of cavities in an aerodynamic flow", WADD-TR-61-75, Wright-Patterson AFB, Dayton, OH, (1962)

2. J.E. Rossiter, "Wind-tunnel experiments on the flow over rectangular cavities at subsonic and transonic speeds", Aeronautical Research Council Reports and Memoranda, Nº 3438, London, (1964)

3. C.B. Burroughs and D.R. Stinebring, "Cavity flow tones in water", *J. Acoust. Soc. Am.*, **95**, 1256-1263, (1994)

4. G.A. Bres and T. Colonius, "Three-dimensional instabilities in compressible flow over open cavities", *J. Fluid Mech.* **599**, 309-339, (2008)

5. X. Gloerfelt, "Cavity noise", Chapter 0, VKI Lectures: Aerodynamic noise from wall-bounded flows, Von Karman Institute, (2009)

6. W. Koch, "Acoustic resonances in rectangular open cavities", AIAA Journal **43**, 2342-2349 (2005)

7. S. Hein, W. Koch and J. Schöberl, "Acoustic resonances in a 2D high lift configuration and 3D open cavity", 26th AIAA Aeroacoustics Conference, Monterey, USA, , paper 2005-2867, (2005)

8. M. Vörlander, "Auralization of spaces", *Physics Today* June, 35-40 (2009)

9. J.B. Allen and D.A. Berkley, "Image method for efficiently simulating small-room acoustics", *J. Acoust. Soc. of Am.*, **65**, 943-950 (1979)

10. J.S. Suh and P.A. Nelson, "Measurement of transient response of rooms and comparison with geometrical acoustic models", *J. Acoust. Soc. of Am.*, **105**, 2304-2317 (1999)

11. J. Berenger, "A perfectly matched layer for the absorption of electromagnetic waves", *J. Comp. Phys.*, **114**, 185–200 (1994)

12. W. E. Arnoldi, "The principle of minimized iterations in the solution of the matrix eigenvalue problem", Quarterly of Applied Mathematics **9**, 1729 (1951)

13. Y. Saad, "Numerical Methods for Large Eigenvalue Problems", SIAM. Minneapolis (1992)

14. F.P. Mechel, “Improved mirror source method in room acoustics”, *J. Sound Vib.*, **256(5)**, (2002).

15. A. Chandak, L. Antani, M. Taylor and D. Manocha, “FastV: From-point Visibility Culling on Complex Models”, *Eurographics Symposium on Rendering*, **28(4)**, (2009).

16. P. Cobo, A. Fernandez and M. Cuesta, “Measuring short impulses responses with inverse filtered Maximum-Length Sequences¨, *App. Ac.*, **56**, (2007)

Table 1 – Eigenvalue results for an Open Cavity (L,D,W)=(53, 38, 32)cm computed with a Helmholtz- PML numerical method.

Mode (n_x, n_y, n_z)	$R_e(k/2\pi)$	$f(Hz)$
(0,0,0)	0,23	151,7
(1,0,0)	0,56	369,4
(0,0,1)	0,86	567,3
(1,1,0)	0,97	639,8
(1,0,1)	0,99	653
(2,0,0)	1,03	679,4
(0,2,1)	1,19	784,9
(1,1,1)	1,3	857,5
(2,0,1)	1,32	870,7
(2,1,0)	1,32	870,7
(3,0,0)	1,53	1009,2
(0,1,1)	1,57	1035,6
(0,0,2)	1,65	1088,4
(1,0,2)	1,72	1134,5
(3,2,0)	1,73	1141,1
(3,0,1)	1,73	1141,1
(0,2,2)	1,86	1226,9
(2,0,0)	1,93	1273,1
(4,0,0)	2,02	1332,4
(2,1,2)	2,11	1391,8

Table 2 – Open Cavity resonant frequencies results. Comparison between measured and numerical simulations. For dimensions (L,D,W)=(53, 38, 32) cm.

Mode (n_x, n_y, n_z)	*Measurements* $f(Hz)$	*Helmholtz* $f(Hz)$	*ISM* $f(Hz)$
(0,0,0)	155	151,7	----
(0,0,1)	568	567,3	548,4
(2,0,0)	673	679,4	665,9
(2,0,1)	843	857,5	858,1
(0,0,2)	1088	1088,4	1088,2
(2,0,2)	1270	1273,1	1268,1

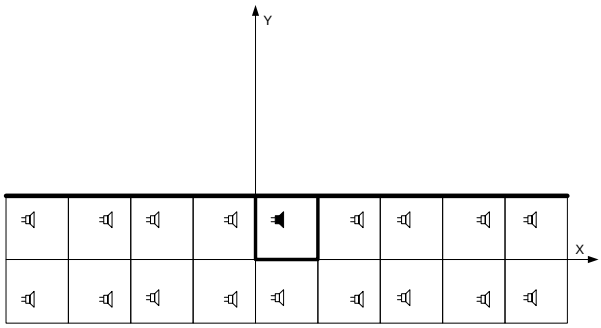

Fig. 1 – 2D Image source space of an open cavity. The box closer to the origin represents the real room.

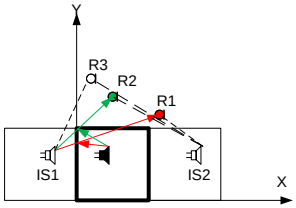

Fig. 2 – Image source validity issues for receivers located outside a rectangular open cavity.

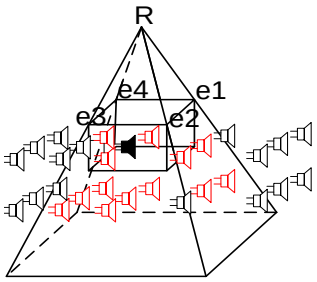

Fig. 3 – Frustum Culling of non-visible IS from a receiver point R located at the apex. Visible IS are marked red, and e1,e2,e3,e4 are the corners of the opening of the cavity.

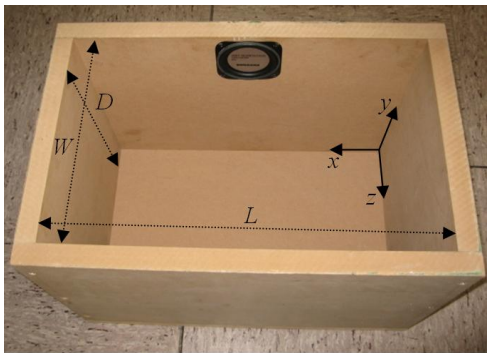

Fig. 4 – The 3D Rectangular Open Cavity.

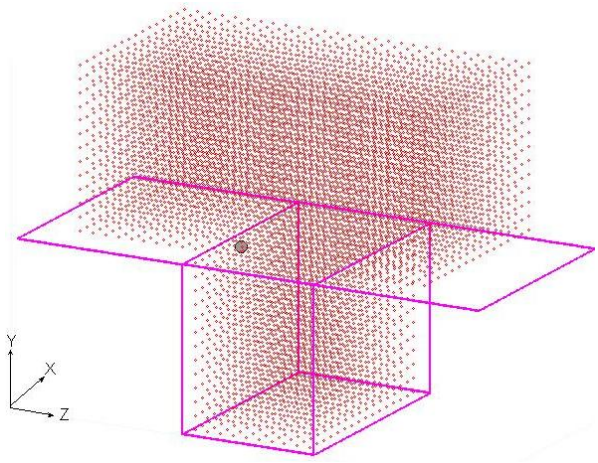

Fig. 5 – Measurement grid inside and outside the open cavity. Red points represent the microphone positions and the grey one stands for the loudspeaker position.

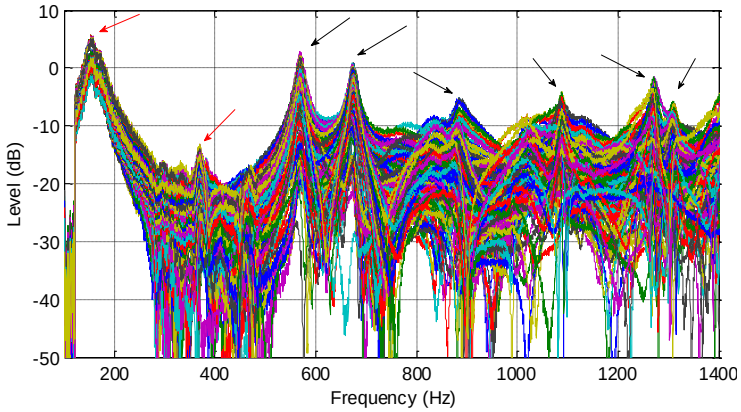

Fig. 6– Frequency Response for 160 Microphone positions. Plane y=0.191 m.

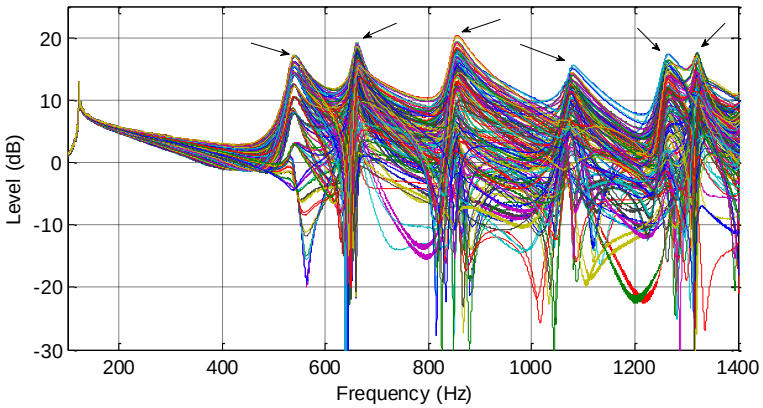

Fig. 7– Frequency Response for Image Source Model Simulation of 160 positions. Plane y=0.191 m.

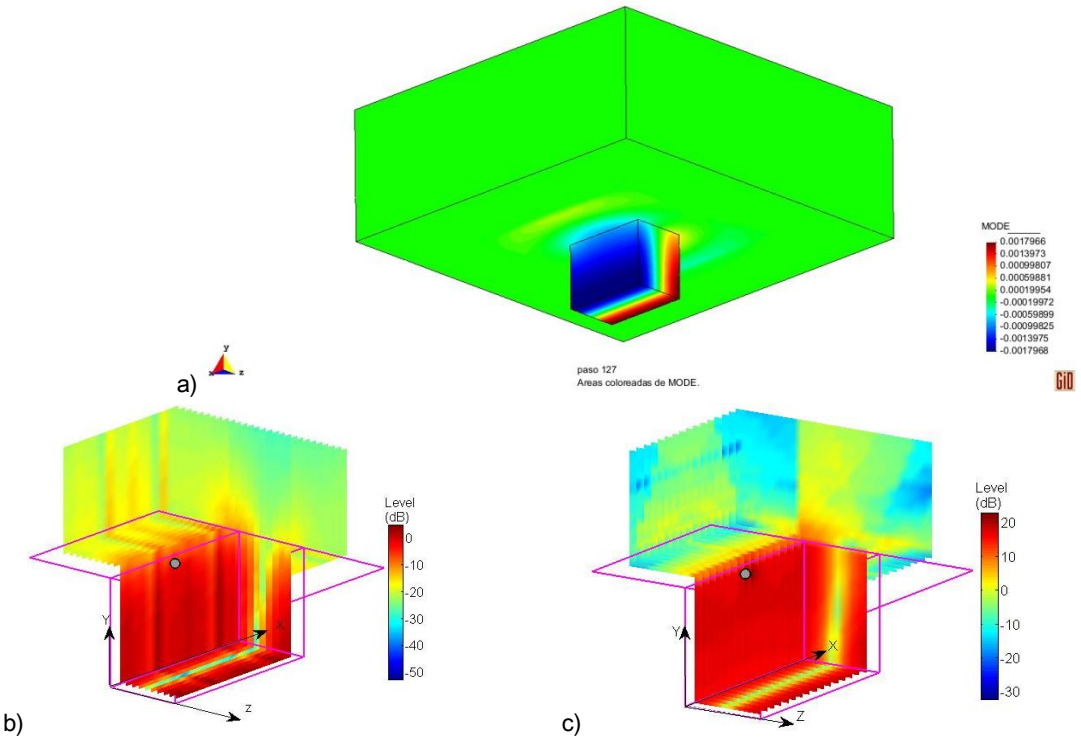

Fig. 8 – Mode (0,0,1). a) Helmholtz-PML b) Experimental Results c) Image Source Model (ISM)

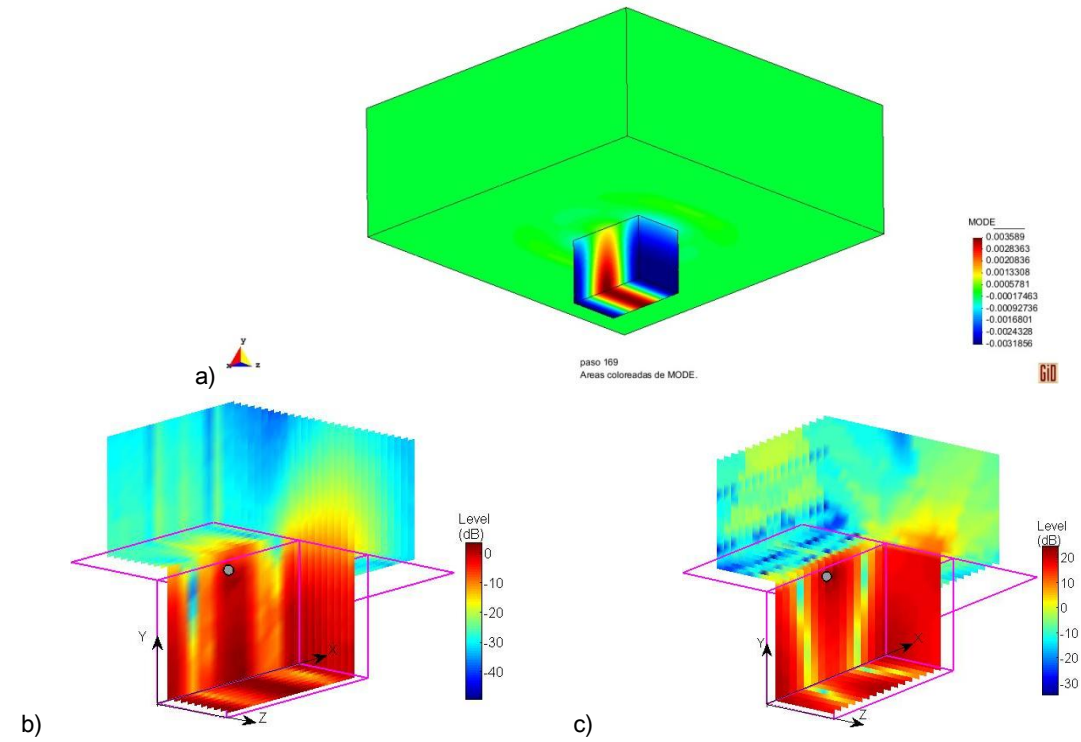

Fig. 9 – Mode (2,0,0). Helmholtz-PML b) Experimental Results c) Image Source Model (ISM)